ROYAL SOCIETY OF CHEMISTRY

Covalently linked mercaptoacetic acid on ZrO$_2$ coupled cellulose nanofibers for solid phase extraction of Hg(II): experimental and DFT studies

Hilal Ahmad, [ID] *[ab] Rais Ahmad Khan [ID] [c] and Ali Alsalme [ID] [c]

Zirconium oxide (ZrO$_2$) nanoparticles were introduced onto cellulose nanofibers after being covalently functionalized with mercaptoacetic acid. We experimentally demonstrate that the nanocomposite is capable of selectively capturing Hg(II) from aqueous samples down to trace level concentrations. Density functional theory (DFT) calculations indicate that energetically favorable R–S → Hg ← O–R bidentate complex formation enhances the rapid adsorption, leading to selective extraction of Hg(II). Furthermore, the loss of ZrO$_2$ particles during flow-through studies is controlled and restricted after binding to CNF rather than being used directly in the column. The Hg(II) selectivity is primarily due to the Lewis soft–soft acid–base chelation of Hg(II) with the mercapto functionalities of the adsorbent. The experimental observations depict a high sorption capacity of 280.5 mg g^{-1} for Hg(II). The limit of detection and quantification of the proposed approach were found to be 0.04 μg L^{-1} and 0.15 μg L^{-1}, respectively. Analytical method accuracy and validity were determined by analyzing Standard Reference Materials and by the standard addition method (recovery > 95% with a 5% RSD). The findings of a Student's *t*-test were found to be lower than the critical Student's *t* value. Real water samples were successfully analyzed using the developed procedure.

Introduction

In recent decades, mercury (Hg(II)) pollution cause from anthropogenic activities has become increasingly prominent in different regions worldwide.[1–3] Anthropogenic behaviors, such as incorrect pesticide application, and industrial and home emissions, were primarily responsible for the accumulation of Hg(II) in the environment.[4,5] Despite the fact that Hg(II) is found in trace levels in diets, it may cause serious health problems after accumulation inside the body for a period of time.[6,7] The toxin dosage and period of exposure all influence the kind and severity of symptoms. Data on the presence of contamination and accumulation rates across a variety of sea foods (fish and sea weeds) might provide crucial insights into the potential human health consequences.[8–10] Mercury poisoning may induce two disorders: Hunter–Russell syndrome and Minamata sickness. "Kawasaki" illness, which is similar to pink sickness and thought to be immunologically mediated, may also be caused by mercury vapor. Long-term mercury exposure damages the brain, kidneys,

and developing fetus irreversibly.[2] Symptoms include sensory impairment, impaired feeling, and a lack of coordination. Inhaling exceedingly large amounts may cause acute pulmonary edema and interstitial pneumonitis, which can be fatal. In non-fatal cases, dyspnea and coughing may continue.[11]

The US Environmental Protection Agency defines the maximum quantity of mercury contamination in drinking water as 2.0 ppb.[12] As a consequence, World Health Organization's top priorities is to monitor and evaluate harmful toxins in the environment.[13,14] Direct detection of Hg(II) at low levels in natural environmental samples using conventional analytical methods is challenging due to significant elemental interferences and sampling restrictions.[14,15] On other side, the spectral interferences are caused by the presence of multiple co-ions at hundreds of times higher concentrations, making it impossible to distinguish the analyte in real samples. As a consequence, sample pretreatment is usually necessary for sample cleanup and increase trace analyte detection accuracy.[16] Among various extraction techniques, in order to attain high enrichment factors and 100% analyte recovery, solid phase extraction (SPE) is the most extensively used, easy to operate, and cost-effective sample preparation technique.[17] Several SPE sorbents, including nano-sorbent, have been successfully characterized for the separation, measurement, and detection of heavy metal ions.[17–20] SPE has been shown to be possible with adsorbents such as graphene oxide, carbon nanotubes, silica, and various composites.[21–25] However, new sorbents must be devised when

[a]Division of Computational Physics, Institute for Computational Science, Ton Duc Thang University, Ho Chi Minh City 700000, Vietnam. E-mail: hilalahmad418@gmail.com

[b]Faculty of Applied Sciences, Ton Duc Thang University, Ho Chi Minh City 700000, Vietnam

[c]Department of Chemistry, College of Science, King Saud University, Riyadh-11451, Kingdom of Saudi Arabia

sample complexity grows and the requirement for selective analysis raises, with faster analysis and higher recovery rate.[26]

The zirconium oxide (ZrO_2) nanoparticles has been investigated extensively for its good physiochemical properties.[27–29] However, using nascent ZrO_2 directly in heavy metal extraction has a number of drawbacks, including limited adsorption capacity and a tendency to agglomerate, resulting in poor dispersion.[29] In aqueous conditions, interparticle interaction causes ZrO_2 to stack, and reducing its adsorption ability. In order to deploy nanostructures effectively, agglomeration/stacking must be avoided.

In this work, considering the rough surface of ZrO_2 with porous topologies, a large surface area and a large number of surface active sites, we chemically functionalized the ZrO_2 nanoparticles with sulfur containing mercaptoacetic acid chelating ligand. The functionalized ZrO_2 nanoparticles was further immobilized onto the cellulose nanofibers (CNF) to provide a solid support. The straightforward *in situ* hydrothermal process for simultaneous functionalization and immobilization of ZrO_2 nanoparticles onto CNFs is described. The solid cellulose nanofiber material firmly retains ZrO_2 and prevents nanoparticle stacking and leaching and simultaneously provides suitable hydrophilicity for effective column operation due to presence of oxygen rich surface functional groups. The presence of thiol groups functionality offers a well-defined site for Hg(II) chelation, which increases Hg(II) adsorption selectivity, while the carboxylic groups of cellulose nanocomposite material increase hydrophilicity, resulting in fast mass transfer. The Hg(II) adsorption measurement was performed on the produced thiol functionalized ZrO_2–CNFs nanocomposite material (abbreviated as C@Zr@TGA sorbent). The prepared C@Zr@TGA sorbent shows selective extraction of Hg(II) over other heavy metals in competitive experimental conditions. The C@Zr@TGA was used to preconcentrates trace Hg(II) from real samples using the column approach.

Experimental

Reagents and synthesis

Nascent ZrO_2 and mercaptoacetic acid (thioglycolic acid AR grade) were purchased from Sigma-Aldrich (Germany). A 1000 ppm stock solution of ($Hg(NO_3)_2$) was obtained from Sigma-Aldrich and utilized after successive dilution. Other metal salts, ethanol, acetone, sulfuric acid, nitric acid, hydrochloric acid, sodium hydroxide, and potassium hydroxide pellets were purchased from Fisher Scientific (India). Cellulose nanofibers was purchased from Biocrown Biotechnology (China) and used after sequential rinsing with HNO_3 (5%), acetone and deionized water. All glass wears were dipped in 1% HNO_3 and rinsed with deionized water (DI) before use. The calibration standards for ICP-OES was obtained from Perkin Elmer, China.

A 5 mL of thioglycolic acid was diluted with 10 mL of deionized water and mixed well. The prewashed ZrO_2 nanoparticles (0.5 g) and cellulose nanofibers (2 g) was dispersed in 20 mL of DI under bath sonicator for 1 h to produce a uniform suspension. The two precursor solution were then mixed and poured into a 100 mL Teflon-lined hydrothermal assembly along with cellulose nanofibers and placed in a muffle furnace at 80 °C for 12 hours. After cooling, the cellulose nanofibers modified with thiol functionalized ZrO_2 nanoparticles were filtered and washed with distilled water several times before being dried in a vacuum oven at 60 °C. The samples were then characterized for surface elemental composition and applied for Hg(II) adsorption studies. Fig. 1 represents the schematic diagram of the synthesis of C@Zr@TGA sorbent.

Experimental procedure

The C@Zr@TGA sorbent was packed into a glass column that had a diameter of 1 cm and a length of 10 cm. The column bed was saturated with a buffer solution of pH 6.0. Sample volumes of 100 mL of known concentrations of Hg(II) were pumped through the column at a rate of 6 mL min^{-1}. The sample flow was controlled by a peristaltic pump. Thereafter, the column was flushed with DI water to remove any unsorbed ions. In order to quantify the adsorbed Hg(II) concentration, the sorbed metal was eluted *via* 5 mL of 1.0 M HNO_3 as a stripping agent and the eluent was analyzed by inductively coupled plasma optical emission spectrometer (ICP-OES, PerkinElmer Avio 200) to quantify the Hg(II) concentration.

Characterization

The surface structure of nascent and modified cellulose nanofibers was studied using a field emission scanning electron microscope (FESEM, JSM-7800F, JEOL, Japan). The solid sample was placed on a sample holder, and a carbon coating was applied. X-ray photoelectron spectra was recorded to observe the elemental composition of prepared adsorbent (XPS; Thermo ESCALAB 250XI), with monochromatic Al Kα excitation at 1486.6 eV and an incident angle of 90°. The model Flash EA 1112 Organic Elemental Analyzer (Thermo Fischer Scientific) was used to carried out the elemental analysis. The concentration of Hg(II) ions was measured using ICP-OES with an ultrasonic nebulizer and a charge-coupled detector in the axial mode of viewing plasma.

Computational method

All calculations were performed using the Gaussian 09 software package. Geometry optimizations was performed by B3LYP command with 6-311G++(d,p) basis set for structural and vibrational parameters, without symmetry restrictions.[24] Energy minimization was performed by density functional calculations using the double numerical plus polarization basis set. Core electron treatment included all electron relativistic options. The same basis set was utilized for chemical stability, bond lengths, stabilization energies and binding energies calculations considering water as a solvent. The LANL2DZ basis set was used to calculate Hg(II) interaction with the prepared sorbent. The solvent effect was simulated by the conductor polarizable continuum model (CPCM).

Results and discussions

Characterization

Fig. 2 depicts the surface morphology of nascent cellulose nanofiber and the produced C@Zr@TGA sorbent, respectively.
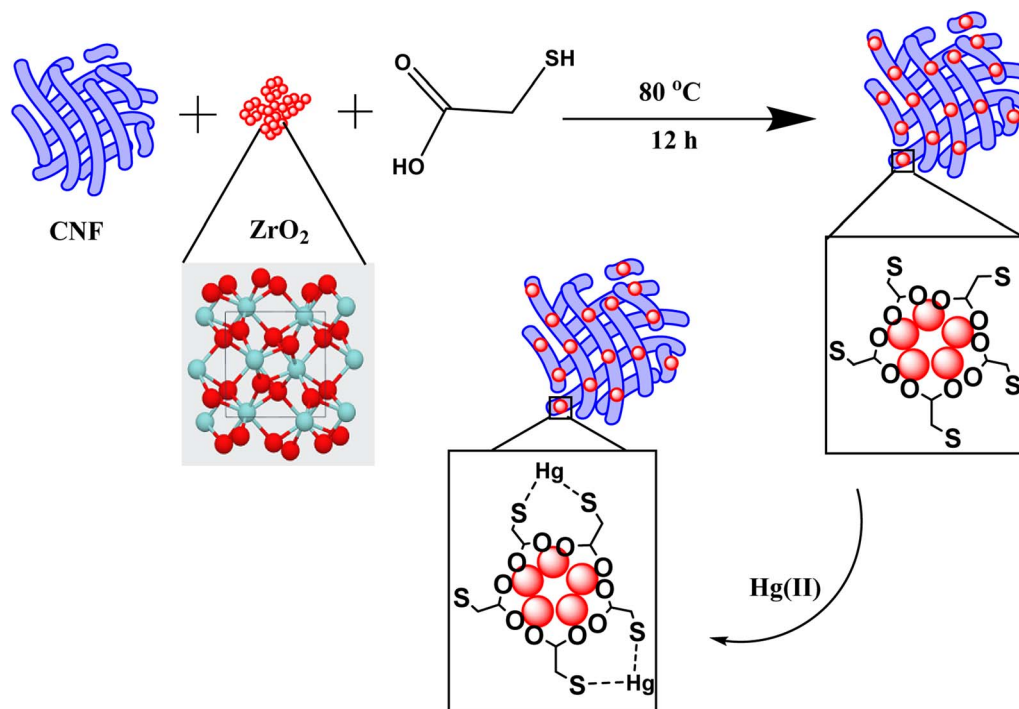
Fig. 1 Schematic representation of synthesis and chelate formation of C@Zr@TGA sorbent.

The effective integration of ZrO_2 nanoparticles into the fiber surface is shown in the FESEM image of the C@Zr@TGA sorbent (Fig. 2B), which is noticeably different from the surface of nascent nanofibers (2A). The XPS analysis was further investigated to observe the inclusion of functionalized ZrO_2 onto the cellulose fiber. The peaks for S ($2p_{3/2}$ and $2p_{1/2}$) observed at the position (BE) of 163.6 eV and 164.7 eV, respectively; were for mercapto (S) groups of the C@Zr@TGA sorbent. Similarly, the peaks observed at 185.7 eV and 183.7 eV for Zr ($3d_{3/2}$ and $3d_{5/2}$) were attributes to ZrO_2 nanoparticles of the C@Zr@TGA sorbent (Fig. 2C and D). The presence of these characteristic peaks depicts the successful preparation of C@Zr@TGA sorbent. The elemental analysis depicts the percentage composition of constituent elements of C@Zr@TGA sorbent and was obtained as C (40.20), H (2.65), N (0.0), O (30.42) and S (2.48). From the % S content data, the amount of TGA (ligand) molecules linked (L_0; mmol g^{-1}) onto the C@Zr@TGA sorbent was estimated using the equation[30] $L_0 = (\% \text{ S/sulfur atomic weight}) \times 10$; and found to be 0.77 mmol g^{-1}. Correlating this with experimental Hg(II) uptake capacity (0.8 mM g^{-1}), it may be concluded that, possibly one –S sites is associated with one Hg(II) to form chelate, which is in accordance with the theoretical observations also.

Optimized experimental variables

The experimental parameters are optimized using a univariate technique, and are detailed below.

Sample pH

The sample pH is an important parameter to tune since it affects metal ion dissociation in aqueous settings. The influence of solution pH on Hg(II) adsorption was investigated utilizing C@Zr@TGA sorbent at pH ranges of 1 to 7. The effects of concomitants administered alongside have also been investigated. Hg(II) adsorption studies at basic pH values were avoided due to the formation of precipitates in the basic media. The adsorption of Hg(II) on unmodified CNF was tested as a control. A 0.25 g of C@Zr@TGA sorbent was shaken with a 50 mg L^{-1} Hg(II) solution for 3 hours (100 mL). The leftovers was then pipetted, and used to measure the concentration of Hg(II) in the supernatant by ICP-OES. Fig. 4A depicts the simulated data. When compared to C@Zr@TGA, the sorption of Hg(II) by nascent CNF remained ineffective at all pH levels. The C@Zr@TGA depicts a potential applicability in the adsorption of Hg(II). Furthermore, when the pH of the solution rise from 2 to 5, Hg(II) sorption improves and reaches a plateau at pH 7. This is owing to the nanocomposite material's exceptionally preferential soft–soft correlations in between Hg(II) and –SH groups.[31,32] The thiol groups of C@Zr@TGA might well be employed as chelate adsorption sites since they have a strong affinity for Hg(II) sorption. However, these binding sites got protonated and poorly sorbed the Hg(II) in extremely acidic conditions, resulting in limited Hg(II) sorption. On the other hand, the association here between thiol groups and H+ weakens as the pH of the sample rises, resulting in increased Hg(II) binding at higher pH levels. Because of the significant number of thiol groups functionalized ZrO_2 with small particle size on the nanofibrous material surface, C@Zr@TGA has a significant sorption tendency for Hg(II). The most likely process for Hg(II) sorption, is the complexation of Hg(II) with the sorbent's thiol groups, together with electrostatic interaction. We also looked at interferences caused by co-existing ions,
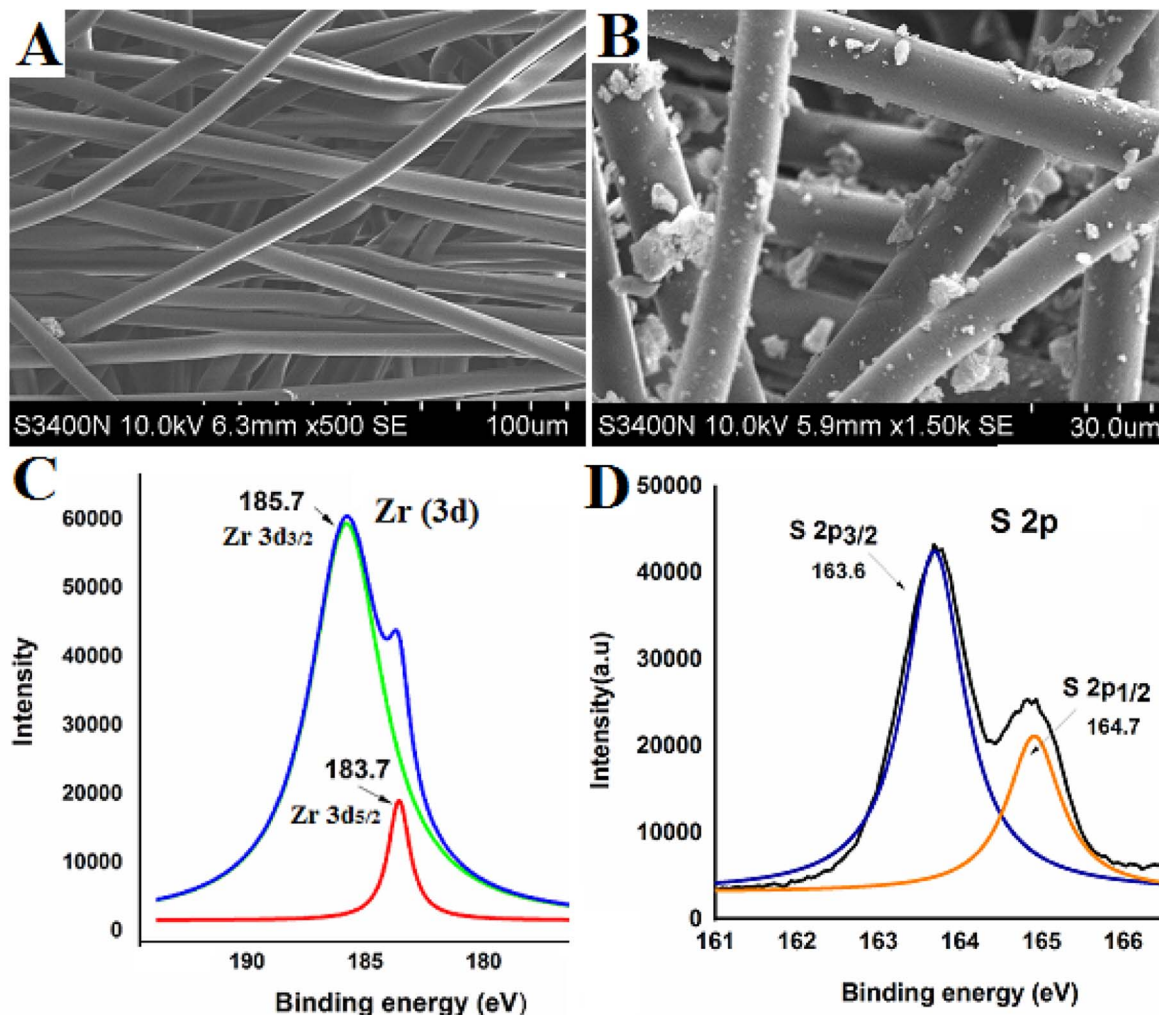
Fig. 2 (A and B) SEM images of nascent and modified CNF; (C) deconvoluted XPS spectra of S and (D) is deconvoluted XPS spectra of Zr elements of prepared C@Zr@TGA sorbent.

Table 1 Effect of foreign ions on the recovery of Hg(II)

Foreign ions	Concentration ($\mu g\ L^{-1}$)	Hg(II) recovery (%)	RSD
Cl^-	7.6×10^3	100	2.86
Br^-	8.2×10^3	97	3.76
PO_4^{--}	2.1×10^2	98.0	4.28
NO_3^-	3.0×10^3	98.7	3.50
SO_4^{--}	2.3×10^3	100.0	3.97
Na^+	5.0×10^4	99.0	3.81
K^+	4.0×10^4	100.2	2.68
Ca^{++}	8.0×10^3	100.1	2.14
Mg^{++}	1.0×10^3	99.4	2.83

which are frequently detected with analyte ions, up to the point where a 5% difference in the emission intensity of pure analyte ions was seen. The results are presented in Table 1. There was no substantial reduction observed in Hg(II) sorption/recovery,

upon the addition of common ions such as Na^+, K^+, Ca^{2+}, Mg^{2+}, Cl^-, Br^-, NO_3^{2-}, SO_4^{2-}, and PO_4^{2-} at five thousand fold concentration.

Computational studies

The optimized structures of ligand and metal chelated ligand with their structural parameters are presented in Fig. 3A–D. It is assumed that the chelating ligand forms two possible coordination spheres with metal ions by one –COOH and one –SH group of single ligand (complex **1**) OR by two –SH groups of two ligands (complex **2a** and **2b**). The calculated thermodynamic data obtained for Hg(II) chelation with the glycine ligand of C@Zr@TGA sorbent are shown in Table 1. Comparison associated with the bond length of metal free and metal affiliated ligand complexes reveals that the C–O and C–S bond distances of C@Zr@TGA sorbent varies upon metalation (complex formation) (Table 2). The obtained data suggest that, among complex **1** and **2**, Hg(II) forms stronger complexes with S–Hg–O, rather than S–Hg. Moreover in complex **1**, the S–Hg and O–Hg
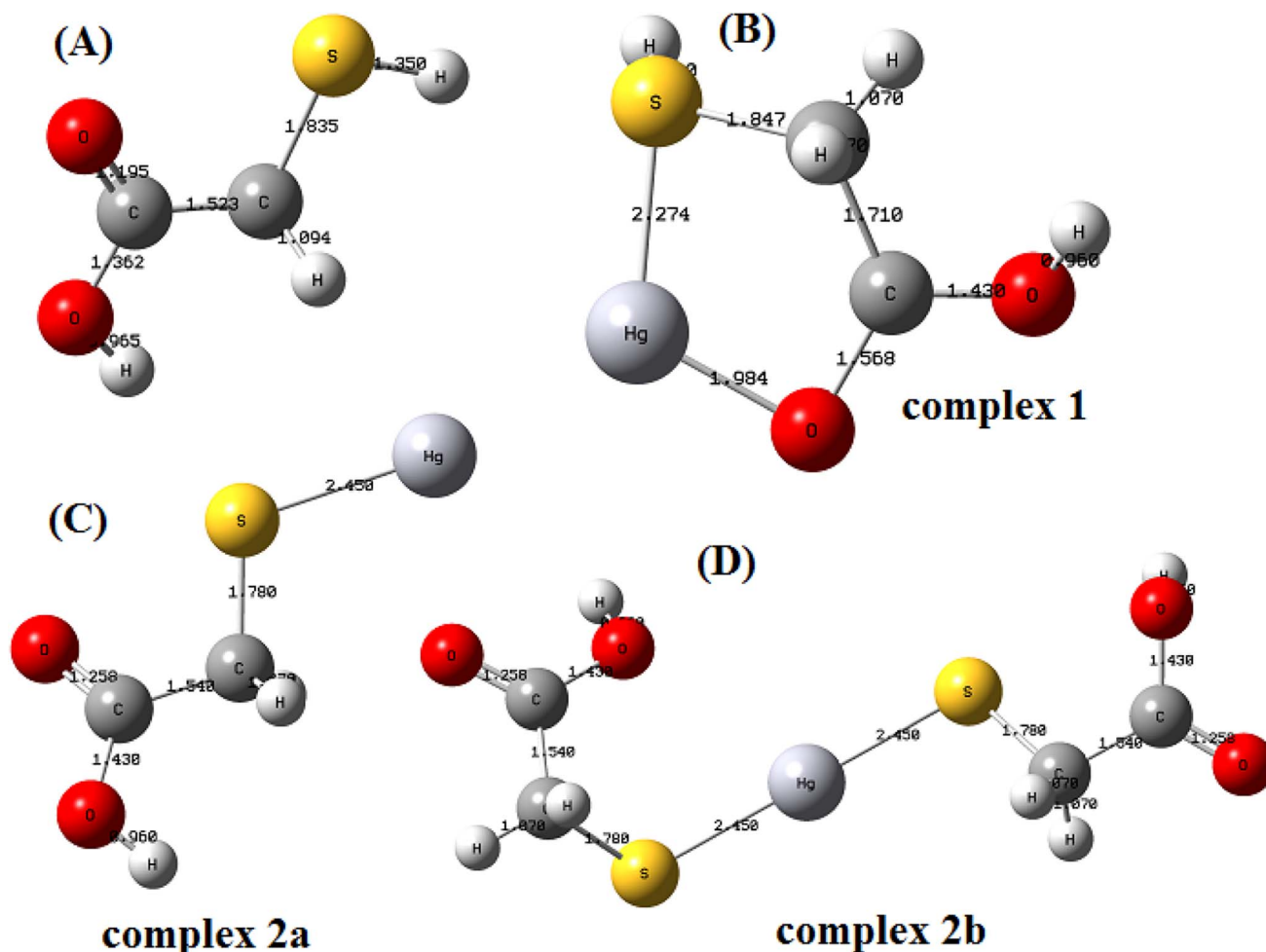
Fig. 3 Optimized structures of (A) nascent ligand and (B) Hg(ɪɪ) chelated complex **1**; (C) Hg(ɪɪ) chelated complex **2a** and (D) Hg(ɪɪ) chelated complex **2b**.

Table 2 Calculated binding energies and thermodynamic parameters (in kcal mol^{-1}) of the Hg(ɪɪ) complex ligand

	ΔG	ΔH
Complex **1**	−47.573	−37.27
Complex **2**	−45.34	−35.62

distances are 2.274, and 1.984 Å, respectively, which is less than those of S–Hg distance (2.450 Å) in complex **2**. This indicates that the interaction between Hg(ɪɪ) and ligand (of C@Zr@TGA sorbent) in complex **1** is stronger than complex **2**. It is concluded that the thiol groups along with oxygen (complex **1**) has high affinity for metal ion complexation and act as primary metal ion binding sites in C@Zr@TGA sorbent than only thiol group.

Sample flow rate optimization

The column flow rate determines not only the equilibrium establishment in between the metal ion and the functional groups, but also the analysis time, in the sorption of Hg(ɪɪ). In

general, optimum sample flow rate allows significant interaction between the chelating groups of the sorbent bed and the metal ions for effective extraction. The impact of the adsorption flow rate on the preconcentration of Hg(ɪɪ) was investigated by flowing a model solution (100 mL) containing 10 ppb of Hg(ɪɪ), maintained at pH 6.0, at a flow rate of 2–8 mL min^{-1}. At 6 mL min^{-1} flow rate, complete adsorption of Hg(ɪɪ) was observed to occur (99.9%). At increasing flow rates, the adsorption percent gradually decreased to 90% and 82%, respectively, at flow rates of 7 and 8 mL min^{-1} (Fig. 4B). As a result, a 6 mL min^{-1} sample flow rate was adjusted and used in the remaining tests.

Selection of eluent

It is necessary and desirable to completely elute out the uptaken analyte ions from the column bed in order to regenerate C@Zr@TGA packed column for the next adsorption cycle. This can be done efficiently with the right choice of eluting agent. To check the most effective eluent, several eluting agents (mineral acids) were tried at different concentration range of 0.25 M to 1.0 M with varying volumes of 2 mL, 3 mL, and 5 mL (Fig. 5). It
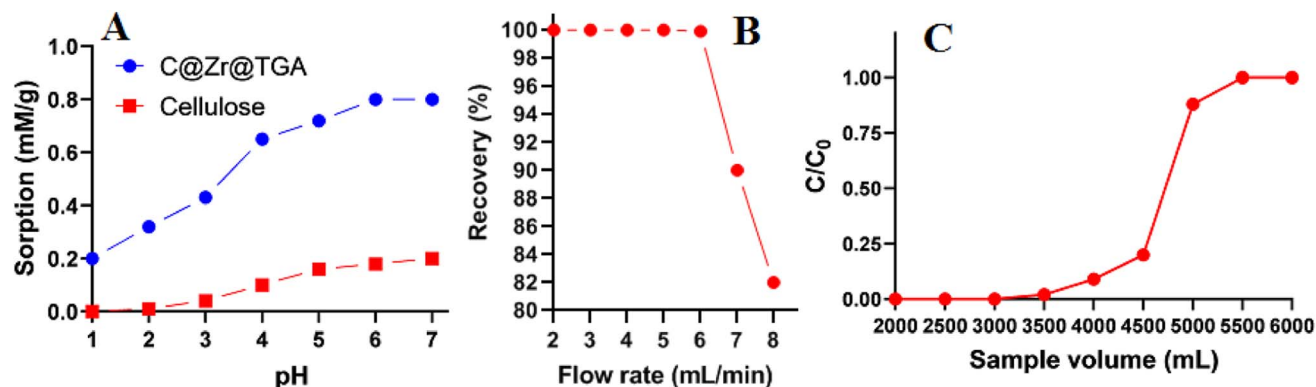
Fig. 4 (A) Effect of sample pH on Hg(II) adsorption by cellulose nanofibers and C@Zr@TGA sorbent (sorbent amount 0.25 g; sample volume 100 mL; Hg(II) 50 mg L^{-1}); (B) effect of column flow rate on Hg(II) recovery (sorbent amount 0.25 g; sample volume 100 mL, Hg(II) 10 µg L^{-1}, sample pH 6.0); (C) breakthrough studies of C@Zr@TGA sorbent (sorbent amount 0.25; sample pH 6.0; Hg(II) 10 mg L^{-1}).

was observed that eluents with high concentration and volumes, quantitatively elutes the Hg(II). While low eluent concentrations, such as 5 mL of 0.5 M HCl and HNO$_3$ gives only 78 and 82% of Hg(II) recovery. As a consequence, 5 mL of 1 M HNO$_3$ was optimized and utilized as the eluting agent to renew the adsorbent for the next sorption cycle.

Studies on preconcentration and breakthrough volume

Determining trace Hg(II) ions in dilute samples using sensitive analytical instrumentation is still challenging due to ultra-trace concentration of analytes and the spectral interferences caused by co-ions. To overcome this, preconcentration steps is more frequently employed to preferably improve the analyte concentration by lowering the sample volume and simultaneously removes matrix interferents and therefore enhances the accuracy of data. A bench of sample solutions were prepared by diluting fix amount of Hg(II) at 1.0 µg to 1500 mL (0.71 ppb), 2000 mL (0.55 ppb), 2500 mL (0.42 ppb), 3000 mL (0.36 ppb), 3200 mL (0.31 ppb), and 3500 mL (0.28 ppb). The pH of all samples were kept at 6.0. All sample solution were passed through the packed column under optimized conditions using peristaltic pump (flow rate 6 mL min^{-1}). The adsorbed amount

of Hg(II) was eluted with 5 mL of stripping agent and subsequently determined by ICP-OES. It is observed that the Hg(II) was quantitatively preconcentrated up to a sample volume of 3200 mL. The analytical recovery of Hg(II) from 3200 mL of sample solution was found to be 99.9%. For an increased sample volume of 3500 mL, the Hg(II) recovery was reduced to 90.0%. To analyse the precision, the same procedure with a sample volume of 3200 mL was repeated for additional numbers of experiments ($N = 3$), and the observed mean recovery value was found to be 99.5% with relative standard deviation (RSD) of 3.42%. The calculated preconcentration limit and preconcentration factor for Hg(II) were 0.31 ppb and 640, respectively.

The breakthrough studies was conducted by percolating a sample volumes ranging from 2000 mL to 6000 mL, containing 10 mg L^{-1} of Hg(II), under optimized experimental conditions. At suitable time intervals, a fractions of effluent was collected and analyzed for amount Hg(II) concentration. The volume at which the Hg(II) concentration in effluent fraction was 3–5% of the loading concentration, was corresponds to the breakthrough volume (Fig. 4C). The comparison of breakthrough capacity (0.80 mM g^{-1}) and the maximum adsorption capacity (0.74 mM g^{-1}) estimated after equilibrating the
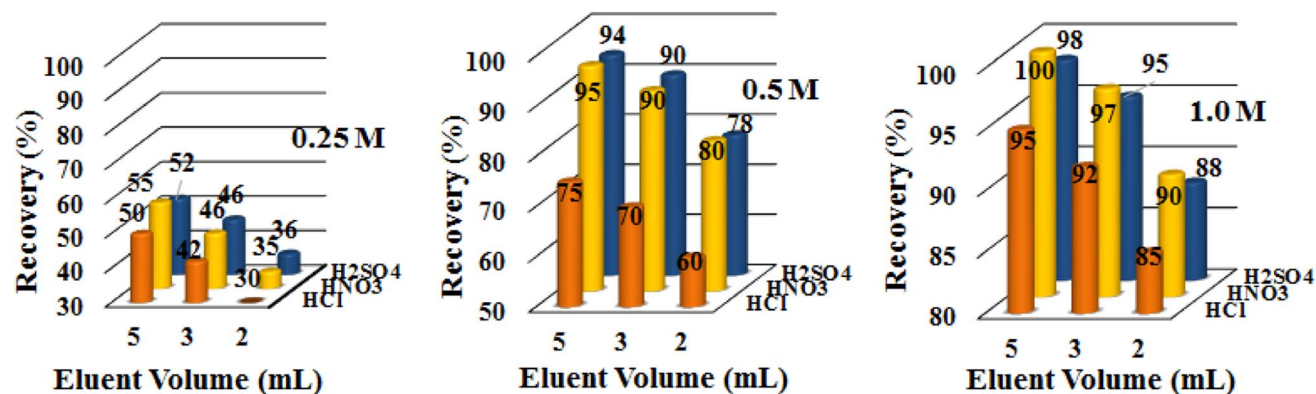

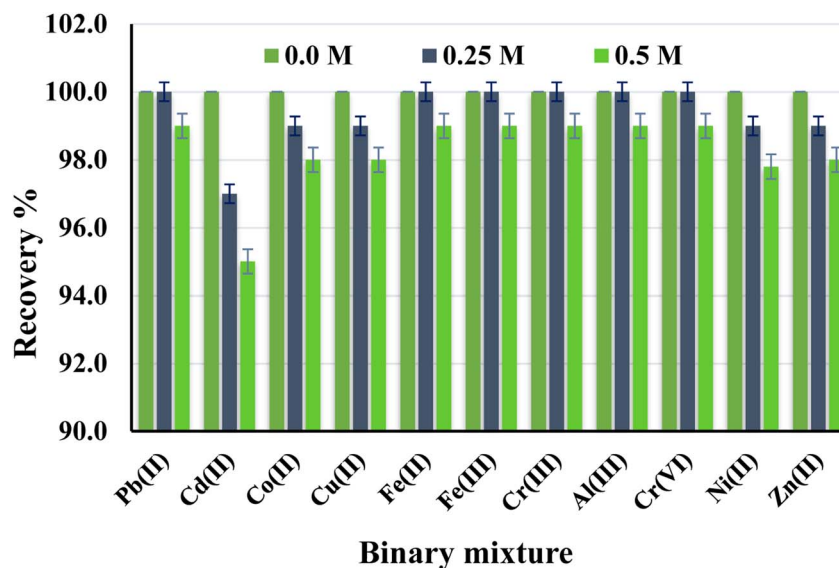Fig. 5 Optimization of eluent (0.25 M, 0.5 M and 1.0 M of HCl, HNO$_3$ and H$_2$SO$_4$).

Fig. 6 Selectivity studies of Hg(II) from varying co-existing ions at 0.25 and 0.5 M concomitant concentration (Hg(II) = 10 µg L^{-1}, sample volume 100 mL).

chelating sites are found closer and suggests the suitability of prepared adsorbent's in column operation.

Selective extraction of Hg(II)

Extracting a 10 µg L^{-1} of Hg(II) from a sample of two component mixtures was used to conduct selectivity tests. The Hg(II) was percolated to a column containing co-ions (such as divalent ions of Zn, Pb, Cd, Cu, and Ni at concentrations of 0.25 M and 0.5 M (sample volume 100 mL)). The concentration of Hg(II) was determined using ICP-OES after the adsorbed Hg(II) was eluted. The results are summarized in Fig. 6. The toleration limit was set at the greatest quantity of co-ion that resulted in a change in Hg(II) enrichment of less than 5%. With an analyte recovery rate of 95–100 percent, there were no significant interferences in the adsorption and detection of Hg(II) for all added ions. The sorption of other competing ions by the C@Zr@TGA sorbent is negligible under optimal circumstances, showing that Hg(II) is selectively absorbed over other divalent metal ions. The Hg(II) complexation with the phosphonate ligands of the C@Zr@TGA adsorbent might explain the Hg selectivity (II). Finally, under better experimental circumstances, selective extraction of Hg(II) from complicated sample matrix may be produced for quantitative measurement.

Validation of analytical methods

Determination of Hg(II) in Standard Reference Materials and the recovery experiments for spiked amount of analyte were conducted to verify the suggested approach. To observe a linearity of the proposed method, calibration plot was obtained in the concentration range of 0.2 to 100 µg L^{-1} of Hg(II) using ICP-OES. The calibration plots (for six data points at 0.2, 5, 25, 50, 75 and 100 µg L^{-1}) was determined to be linear, with R^2 value of 0.9998. The methods detection limit (LOD) and limit of quantification (LOQ) were estimated using the IUPAC criteria as

Table 3 Structural parameters of ligand and Hg(II) complex

	C–O (Å)	C–S (Å)	Hg–S (Å)	Hg–O (Å)
Ligand	1.195	1.835	—	—
Complex **1**	1.568	1.847	2.274	1.984
Complex **2**	1.258	1.780	2.450	—

three times and ten times the standard deviation of mean blank signals obtained after 11 consecutive blank measurements, respectively.[33] The LOD and LOQ were calculated to be 0.05 µg L^{-1} and 0.20 g L^{-1}, respectively, suggesting the suitability for trace Hg(II) determination in real-world samples. Ten successive measurements of 1 µg L^{-1} of Hg(II) were taken to examine accuracy, and the relative standard deviation was determined to be 3.5%, demonstrating that repeated observations may be relatively close. The accuracy of the developed approach, *i.e.* the closeness of the agreement between the results of a measurement and a true value, was examined and confirmed by evaluating the SRM 1641d and the water samples after spiking Hg(II) (known) concentrations. The data for the spiking quantity of

Table 4 Validation of the proposed methodology for the analysis of Hg(II) ions

Samples	Certified values (µg g^{-1})	Values found by proposed method^a (µg g^{-1}) ± standard deviation	Value of t-test^b
NIST SRM 1641d^c	1.56 ± 0.020	1.541 ± 0.480	1.283

^{a} Mean value, $N = 3$. ^{b} At 95% confidence level. ^{c} Ampoules were opened immediately before use by breaking the glass at the score line in the narrowest segment of the neck of the ampoule.

Table 5 Determination of Hg(II) in real samples after solid phase extraction using packed column

Samples	Amount added (μg)	Hg(II) found (μg L^{-1}) ± standard deviation[a]	Recovery percent of added amount[c] (RSD)	Value of t-test[d]
Tap water	0	ND[b]	—	—
	3	3.01 ± 0.25	100.3 (0.25)	0.80
	5	4.95 ± 0.55	99.0 (0.35)	1.59
Lake water	0	3.50 ± 0.43	—	—
	3	6.53 ± 0.92	100.4 (0.43)	1.52
	5	8.50 ± 0.98	100 (0.56)	1.21
Ground water	0	1.50 ± 0.73	—	1.49
	3	4.52 ± 0.58	100.4 (0.36)	1.18
	5	6.50 ± 0.68	100 (0.59)	1.24

[a] $N = 3$. [b] Not detected. [c] Relative standard deviation. [d] At 95% confidence level, $t_{critical} = 4.303$.

Table 6 Comparative Hg(II) adsorption/preconcentration data of C@Zr@TGA sorbent with previous reports

Sorbent	Sorption capacity (mg g^{-1})	Preconcentration factor	Detection limit (μg L^{-1})	Ref.
C@Zr@TGA	160.5	640	0.05	This work
Cellulose/CdS	126.0	580	0.06	34
Cellulose/PEI	247.5	—	—	35
Fe$_3$O$_4$@SiO$_2$SH	132	120	—	36
Fe$_3$O$_4$/graphene oxide	128.0	—	0.25	37

Hg(II) retrieved in the range of 97.5–100% and are summarized in Table 3. The proximity between the observed and referred values for Standard Reference Materials in Table 2 shows the procedure accuracy at a 95% confidence level. Furthermore, the adsorption elution findings are stable up to 40 cycles, after which there is an 8% reduction in recovery percent. As a result, the proposed column procedure may be used several times for adsorption tests (Tables 4 and 5).

Conclusion

Inorganic–organic interfaces play a very important role in mechanical properties, phase separation and the interactions between analyte and matrix. Customizing the particle surface is therefore crucial for technological development. In this research, we describe a new CNF composite immobilized with, thioglycolic acid manipulated zirconia nanoparticles. *In situ* nanocomposite synthesis was achieved by hydrothermal reaction combining zirconia nanoparticles and thioglycolic acid with the CNF formulation. The organic ligand's bound zirconia surface, resulting in thiol functionalized metal oxide nanoparticles, are used to adorn cellulose nanofibers. SEM and XPS measurements were used to look into the distribution and functionalization of nanoparticles. From complicated sample matrices, the developed SPE material demonstrates selective Hg(II) adsorption. The thiol group's Lewis hard–soft acid–base interaction with Hg(II) ions leads to highly selective Hg(II) adsorption with no interference from co-existing ions. By looking at SRM and using a traditional spiking (addition) technique, the applicability has been proven. Table 6 summarizes the findings of a previous study comparing the Hg(II) adsorption and preconcentration performance of cellulose-based adsorbents. The properties of this adsorbent are comparable to those of similar adsorbents previously described. Our findings on the utilization of ZrO$_2$ in SPE might pave the way for further research into transition metal oxides as sorbents for environmental monitoring and evaluation. The successful immobilization of ZrO$_2$ nanoparticles onto the surface of nanocomposite materials opens the door to further research into the functionalization of other nanomaterials onto the active surface of nanocomposite materials to reduce fouling in forward osmosis nanocomposite reactors.

Conflicts of interest

All author's declared no conflict of interest.

Acknowledgements

References

1 N. Basu, M. Horvat, C. Evers David, I. Zastenskaya, P. Weihe and J. Tempowski, A State-of-the-Science Review of Mercury Biomarkers in Human Populations Worldwide between 2000 and 2018, *Environ. Health Perspect.*, 2018, **126**, 106001.

2 S. E. Abalaka, S. I. Enem, I. S. Idoko, N. A. Sani, O. Z. Tenuche, S. A. Ejeh and W. K. Sambo, Heavy Metals Bioaccumulation and Health Risks with Associated Histopathological Changes in Clarias gariepinus from the Kado Fish Market, Abuja, Nigeria, *J. Health Pollut.*, 2020, **10**, 200602.

3 Y. Wu, R. Yin, C. Li, D. Chen, S. E. Grasby, T. Li, S. Ji, H. Tian and P. a. Peng, Global Hg cycle over Ediacaran–Cambrian transition and its implications for environmental and biological evolution, *Earth Planet. Sci. Lett.*, 2022, **587**, 117551.

4 S. Osterwalder, J. H. Huang, W. H. Shetaya, Y. Agnan, A. Frossard, B. Frey, C. Alewell, R. Kretzschmar, H. Biester and D. Obrist, Mercury emission from industrially contaminated soils in relation to chemical, microbial, and meteorological factors, *Environ. Pollut.*, 2019, **250**, 944–952.

5 A. J. Adewumi and T. A. D. Laniyan, Contamination, sources and risk assessments of metals in media from Anka artisanal gold mining area, Northwest Nigeria, *Sci. Total Environ.*, 2020, **718**, 137235.

6 J. C. Dabrowiak, Metal ion imbalance in the body, in *Metals in Medicine*, 2nd edn, 2017, Wiley, pp. 329–356.

7 J. Briffa, E. Sinagra and R. Blundell, Heavy metal pollution in the environment and their toxicological effects on humans, *Heliyon*, 2020, **6**, e04691.

8 I. Sioen, S. De Henauw, J. Van Camp, J.-L. Volatier and J.-C. Leblanc, Comparison of the nutritional–toxicological conflict related to seafood consumption in different regions worldwide, *Regul. Toxicol. Pharmacol.*, 2009, **55**, 219–228.

9 O. J. Afonne, J. U. Chukwuka and E. C. Ifediba, Evaluation of drinking water quality using heavy metal pollution indexing models in an agrarian, non-industrialised area of South-East Nigeria, *J. Environ. Sci. Health, Part A: Toxic/Hazard. Subst. Environ. Eng.*, 2020, 1–9.

10 J. d. Souza-Araujo, N. E. Hussey, R. A. Hauser-Davis, A. H. Rosa, M. d. O. Lima and T. Giarrizzo, Human risk assessment of toxic elements (As, Cd, Hg, Pb) in marine fish from the Amazon, *Chemosphere*, 2022, **301**, 134575.

11 Y. Li, C. Lu, N. Zhu, J. Chao, W. Hu, Z. Zhang, Y. Wang, L. Liang, J. Chen, D. Xu, Y. Gao and J. Zhao, Mobilization and methylation of mercury with sulfur addition in paddy soil: Implications for integrated water-sulfur management in controlling Hg accumulation in rice, *J. Hazard. Mater.*, 2022, **430**, 128447.

12 Environmental Protection Agency, 2019.

13 W. H. Organization, *Guidelines for Drinking-Water Quality*, WHO, 4th edn, 2017.

14 U. Haseen and H. Ahmad, Preconcentration and Determination of Trace Hg(II) Using a Cellulose Nanofiber Mat Functionalized with MoS2 Nanosheets, *Ind. Eng. Chem. Res.*, 2020, **59**, 3198–3204.

15 H. Ahmad, I. I. B. Sharfan, R. A. Khan and A. Alsalme, Effective Enrichment and Quantitative Determination of Trace Hg2+ Ions Using CdS-Decorated Cellulose Nanofibrils, *Nanomaterials*, 2020, **10**, 1–11.

16 H. Ahmad, Z. Huang, P. Kanagaraj and C. Liu, Separation and preconcentration of arsenite and other heavy metal ions using graphene oxide laminated with protein molecules, *J. Hazard. Mater.*, 2020, **384**, 121479.

17 C. Zhang, H. Xing, L. Yang, P. Fei and H. Liu, Development trend and prospect of solid phase extraction technology, *Chin. J. Chem. Eng.*, 2022, **42**, 245–255.

18 M. Bilal, I. Ihsanullah, M. Younas and M. Ul Hassan Shah, Recent advances in applications of low-cost adsorbents for the removal of heavy metals from water: a critical review, *Sep. Purif. Technol.*, 2022, **278**, 119510.

19 L. Zhang, J. Zhang, X. Li, C. Wang, A. Yu, S. Zhang, G. Ouyang and Y. Cui, Adsorption behavior and mechanism of Hg (II) on a porous core-shell copper hydroxy sulfate@MOF composite, *Appl. Surf. Sci.*, 2021, **538**, 148054.

20 Z. Xu, Q. Zhang, X. Li and X. Huang, A critical review on chemical analysis of heavy metal complexes in water/wastewater and the mechanism of treatment methods, *Chem. Eng. J.*, 2022, **429**, 131688.

21 C. Li, L. Duan and X. Cheng, Facile method to synthesize fluorescent chitosan hydrogels for selective detection and adsorption of Hg2+/Hg+, *Carbohydr. Polym.*, 2022, **288**, 119417.

22 Y. Zhou, Y. Gao, H. Wang, M. Xia, Q. Yue, Z. Xue, J. Zhu, J. Yu and W. Yin, Versatile 3D reduced graphene oxide/poly(amino-phosphonic acid) aerogel derived from waste acrylic fibers as an efficient adsorbent for water purification, *Sci. Total Environ.*, 2021, **776**, 145973.

23 Y. Wang, J. Chen, H. Ihara, M. Guan and H. Qiu, Preparation of porous carbon nanomaterials and their application in sample preparation: A review, *TrAC, Trends Anal. Chem.*, 2021, **143**, 116421.

24 U. Haseen, S. G. Ali, K. Umar, A. Ali, H. Ahmad and H. M. Khan, Dimercaptosuccinic Acid Functionalized Polystyrene Column for Trace Concentration Determination of Heavy Metal Ions: Experimental and Theoretical Calculation Studies, *Water*, 2021, **13**.

25 M. Khajeh, S. Laurent and K. Dastafkan, Nanoadsorbents: Classification, Preparation, and Applications (with Emphasis on Aqueous Media), *Chem. Rev.*, 2013, **113**, 7728–7768.

26 X. Qian, R. Wang, Q. Zhang, Y. Sun, W. Li, L. Zhang and B. Qu, A delicate method for the synthesis of high-efficiency Hg (II) The adsorbents based on biochar from corn straw biogas residue, *J. Cleaner Prod.*, 2022, **355**, 131819.

27 J. Xu, P. Wu, E.-C. Ye, B.-F. Yuan and Y.-Q. Feng, Metal oxides in sample pretreatment, *TrAC, Trends Anal. Chem.*, 2016, **80**, 41–56.

28 S. Y. Sokovnin, N. Pizurova, V. G. Ilves, P. Roupcová, M. G. Zuev, M. A. Uimin, M. V. Ulitko and O. A. Svetlova, Properties of ZrO2 and Ag–ZrO2 nanopowders prepared by pulsed electron beam evaporation, *Ceram. Int.*, 2022, **48**, 17703–17713.

29 H. Ahmad, R. Ahmad Khan, B. Heun Koo and A. Alsalme, Cellulose Nanofibers@ZrO2 membrane for the separation of Hg(II) from aqueous media, *J. Phys. Chem. Solids*, 2022, **168**, 110812.

30 S. A. Idris, C. M. Davidson, C. McManamon, M. A. Morris, P. Anderson and L. T. Gibson, Large pore diameter MCM-41 and its application for lead removal from aqueous media, *J. Hazard. Mater.*, 2011, **185**, 898–904.

31 R. G. Pearson, The HSAB principle—more quantitative aspects, *Inorg. Chim. Acta*, 1995, **240**, 93–98.

32 R. G. Pearson, Hard and soft acids and bases, HSAB, part 1: Fundamental principles, *J. Chem. Educ.*, 1968, **45**, 581.

33 G. L. Long and J. D. Winefordner, Limit of Detection A Closer Look at the IUPAC Definition, *Anal. Chem.*, 1983, **55**, 712A–724A.

34 H. Ahmad, I. I. B. Sharfan, R. A. Khan and A. Alsalme, Effective Enrichment and Quantitative Determination of Trace Hg^{2+} Ions Using CdS-Decorated Cellulose Nanofibrils, *Nanomaterials*, 2020, 1–11.

35 R. R. Navarro, K. Sumi, N. Fujii and M. Matsumura, Mercury removal from wastewater using porous cellulose carrier modified with polyethyleneimine, *Water Res.*, 1996, **30**, 2488–2494.

36 C. R. Lin, O. S. Ivanova, D. A. Petrov, A. E. Sokolov, Y. Z. Chen, M. A. Gerasimova, S. M. Zharkov, Y. T. Tseng, N. P. Shestakov and I. S. Edelman, Amino-Functionalized Fe(3)O(4)@SiO(2) Core-Shell Magnetic Nanoparticles for Dye Adsorption, *Nanomaterials*, 2021, **11**, 1–10.

37 X. Wang, Z. Zhang, Y. Zhao, K. Xia, Y. Guo, Z. Qu and R. Bai, A Mild and Facile Synthesis of Amino Functionalized $CoFe_2O_4@SiO_2$ for Hg(II) Removal, *Nanomaterials*, 2018, **8**, 1–8.